

Collaborative Threat-Aware Autonomy (CTAA)

Rajnikant Sharma*

Integrated Solutions for Systems Inc. (IS4S), Dayton, Ohio

Abhinav Sinha †

*Guidance, Autonomy, Learning, and Control for Intelligent Systems (GALACxIS) Lab,
Department of Aerospace Engineering and Engineering Mechanics,
University of Cincinnati, Cincinnati, OH, 45221, USA*

Isaac Weintraub ‡

*Autonomous Controls Branch,
Power and Control Division,
Aerospace Systems Directorate,
Air Force Research Lab, Wright-Patterson AFB, OH 45433, USA*

Navigating teams of unmanned vehicles through environments containing dynamic, adversarial Weapon Engagement Zones (WEZs) poses a fundamental challenge to mission success: a single vehicle, however capable its onboard guidance, remains a single point of failure. This paper presents a role-differentiated multi-agent framework for collaborative threat-aware trajectory planning in which a fleet of Autonomous Collaborative Platforms (ACPs) is assigned distinct roles — primary intercept, escort, and decoy — to improve team-level mission success probability while managing individual WEZ exposure. Each ACP independently employs a reactive guidance law derived from the Collision Sphere Boundary for Evader Zero-Set (CSBEZ), which accounts for pursuer maneuverability constraints imposed by minimum turn radius, and steers the vehicle toward the safest heading that also makes progress toward its goal. Role assignment and spatial route separation induce two complementary effects: probabilistic redundancy, in which N independent paths raise the team success probability to $1 - (1 - p)^N$, and threat saturation, in which lower-priority escorts and decoys draw adversary attention and free the primary vehicle to transit uncontested. Simulation results on a two-gate gauntlet scenario demonstrate that the three-vehicle team raises mission success probability from 0.72 (single CSBEZ-aware vehicle) to 0.978, a +35.8 percentage-point improvement. Monte Carlo validation over 100 trials with perturbed threat range, position, and speed yields an empirical team success rate of 1.00 ± 0.00 , against a single-vehicle rate of 0.66 ± 0.09 . Experiments with reactive PurePursuit threats confirm that the decoy-and-protect structure remains effective even when adversaries dynamically re-target the nearest ACP.

I. Introduction

The contested airspace environments anticipated in both Advanced Air Mobility (AAM) and autonomous strike scenarios require unmanned platforms to navigate in the presence of hostile interceptors whose Weapon Engagement Zones (WEZs) dynamically reshape according to their kinematics and sensor geometry [1]. The WEZ defines the region from which an adversarial pursuer, modeled as a turn-constrained Dubins vehicle, can intercept a target within a bounded engagement range. Awareness of the WEZ boundary provides actionable guidance: a vehicle should steer to keep itself outside the capture zone while still making progress toward its mission objective.

Single-vehicle WEZ-aware reactive guidance has been addressed by several recent approaches. Von Moll and Weintraub [2] introduced the Dynamic Maneuvering Cue (DMC), a closed-form risk metric that quantifies the heading change required to exit the current WEZ boundary, and applied it to both a simple feedback controller and a Model Predictive Controller (MPC). Stagg, Weintraub, and Peterson [3] extended this foundation to the Collision Sphere Boundary for Evader Zero-Set (CSBEZ), which replaces the infinite-turn-rate Basic Engagement Zone (BEZ)

*PNT Research Engineer, **email:** rajnikant.sharma@is4s.com (Associate Fellow, AIAA).

†Assistant Professor, **email:** abhinav.sinha@uc.edu (Senior Member, AIAA).

‡Senior Electronics Engineer. **email:** isaac.weintraub.1@us.af.mil (Associate Fellow, AIAA).

with a pursuer constrained to follow a Dubins arc-plus-straight intercept path. The CSBEZ scalar field provides a state-dependent safety margin whose sign directly indicates whether the evader can escape under optimal heading choice.

While these approaches are effective for a single vehicle, they share a common limitation: a single WEZ-aware vehicle still fails with probability $1 - p$ per mission, where p is the individual success rate. In operational scenarios where $p \approx 0.65\text{--}0.75$, mission reliability is insufficient. Multi-vehicle teaming offers a natural path to improved reliability via redundancy, but realizing the theoretical gain requires that the vehicles be assigned roles and routes that prevent the threat from negating all of them simultaneously.

This paper makes the following contributions:

- 1) A role-differentiated multi-ACP framework in which a primary (high value, weight $w = 2$), escort (weight $w = 1$), and decoy (weight $w = 0.5$) each run independent CSBEZ reactive controllers on spatially separated routes.
- 2) A role-weighted team metric suite — cumulative WEZ exposure J_{WEZ} , violation score V_{WEZ} , safety margin m_{team} , and mission success probability P_{mission} — that captures the trade-off between individual risk and team-level outcome.
- 3) Deterministic simulation on a two-gate gauntlet scenario demonstrating a +35.8 pp improvement in P_{mission} over a single CSBEZ vehicle.
- 4) Monte Carlo validation (100 trials) confirming that the empirical team success rate matches the analytical redundancy bound.
- 5) A reactive-threat experiment showing that PurePursuit adversaries are naturally absorbed by escort and decoy, leaving the primary uncontested without any inter-vehicle communication.

II. Related Work

Threat-aware autonomy for contested airspace sits at the intersection of curvature-constrained motion planning, pursuit–evasion and active-defense differential games, engagement-zone modeling, and multi-agent coordination. The existing literature has produced strong foundations for modeling the reachability of adversarial pursuers and for planning safe trajectories for a single vehicle. However, a single vehicle remains a single point of mission failure: if the vehicle must cross a sequence of dynamic WEZs, even a risk-aware planner with high individual success probability can still produce insufficient mission reliability in repeated or uncertain engagements. This motivates the central thesis of this paper: threat-aware autonomy should be formulated not only as an individual path-safety problem, but also as a team-level mission-success problem in which role assignment, route diversity, redundancy, and deliberate threat saturation can improve the probability that at least one mission-critical ACP reaches the objective.

A. Curvature-Constrained Motion and Interception Foundations

A large portion of threat-aware autonomy relies on reachable-set reasoning for vehicles with bounded curvature or turn-rate constraints. Dubins’ classical result characterises shortest paths for forward-moving vehicles with bounded curvature between prescribed configurations [4]. Cockayne and Hall extended this analysis to the reachable positions of a constant-speed particle subject to curvature constraints [5]. These results are directly relevant to WEZ modeling because a pursuer with finite turn radius cannot instantaneously intercept an evader; the shape of the capture region is determined by vehicle kinematics rather than range alone.

Time-optimal interception extends this foundation to moving targets. Buzikov and Galyaev formulated interception of a moving target by a Dubins car as a time-optimal control problem and derived algebraic conditions for the optimal interception time [6]. For threat-aware autonomy, these results imply that a circular keep-out zone is generally inadequate; a physically meaningful engagement zone must account for pursuer heading, speed, finite range, and minimum turn radius.

B. Single-Vehicle WEZ-Aware Planning

Von Moll and Weintraub introduced Basic Engagement Zones (BEZs) as regions of the state space from which a pursuer can intercept a target under specified engagement assumptions [1], moving the field beyond heuristic circular threat regions toward engagement regions derived from the pursuer–evader geometry. Weintraub’s dissertation further developed optimal defense of high-value airborne assets, connecting engagement geometry with active defense and optimal-control formulations [7].

Optimal-control approaches have been applied directly to routing around dynamic engagement zones. Weintraub et

al. posed a two-dimensional engagement-zone avoidance problem in which a vehicle reaches a desired location while trading off WEZ exposure [8]. Dillon et al. extended this to aircraft trajectories avoiding multiple WEZs and showed how keep-out constraints can be incorporated into optimal trajectory generation [9]. To improve scalability, Wolek et al. proposed a sampling-based risk-aware planner in the (x, y, ψ) state space using an RRT*-style search [10], and Milutinović et al. formulated stochastic optimal avoidance of multiple engagement zones with feedback policies in dynamic risk fields [11].

Turn-constrained pursuer models are especially relevant here. Chapman et al. derived engagement-zone models for pursuers with finite turn constraints [12]. Stagg, Weintraub, and Peterson extended these concepts to probabilistic WEZs for a turn-constrained pursuer with uncertain parameters [3]. These works provide the physical and probabilistic basis for the CSBEZ threat model used in the present paper. The remaining gap is not the absence of a single-vehicle risk metric; rather, it is the lack of a team-level autonomy framework that uses these risk fields to coordinate multiple ACPs with different mission values and roles.

C. Active Target Defense and Multi-Agent Pursuit–Evasion

The target–attacker–defender (TAD) literature provides the strongest precedent for explicitly multi-agent threat interactions. Garcia, Casbeer, and Pachter developed cooperative strategies for defending an aircraft from an attacking missile [13]. Weintraub et al. derived optimal aircraft defense strategies for the active-target-defense scenario [14]. Casbeer, Garcia, and Pachter analysed a target differential game with two defenders, demonstrating how additional defenders alter the game structure and winning regions [15].

Multi-player TAD games generalise these ideas to larger teams. Coon and Panagou derived control strategies for multiplayer TAD games with double-integrator dynamics [16]. Manyam et al. studied coordinated defender path planning for an optimal TAD game, highlighting the value of coordinating routes rather than treating defenders independently [17]. Manoharan and Baliyarasimhuni demonstrated that target–defender teams can cooperate in real time using nonlinear model predictive control [18].

However, TAD formulations usually focus on explicit defender interception of attackers or missiles. The ACP problem studied here is different: the friendly vehicles are not tasked with destroying threats. Instead, a team must transit through dynamic WEZs while completing a mission objective, and lower-value vehicles can passively occupy adversarial attention so that a higher-value primary preserves mission success. This creates a bridge between WEZ-aware path planning and active target defense: the team shapes the adversary’s engagement opportunities through route separation and role differentiation.

D. From Single-Vehicle Threat Avoidance to Team-Level Mission Success

The preceding literature reveals three limitations of the current state of the art. First, single-vehicle WEZ-aware planners reduce exposure but cannot remove the single-point-of-failure problem: if the individual success probability is p , the mission still fails with probability $1 - p$. Second, most engagement-zone planners optimise vehicle-level quantities (path length, time, accumulated risk) rather than the team-level probability that at least one mission-critical vehicle succeeds. Third, many multi-agent adversarial-control papers assume explicit defender–attacker roles and direct engagement, whereas practical ACP missions benefit from less communication-intensive mechanisms such as spatial route diversity and role-weighted risk allocation.

This paper addresses these gaps by using CSBEZ risk fields inside a role-differentiated multi-ACP architecture. If vehicle outcomes are approximately independent,

$$P_{\text{mission}}(N) = 1 - (1 - p)^N.$$

For p in the range typical of challenging single-vehicle WEZ transit, this redundancy effect alone is substantial. More importantly, route diversity and role assignment can make the independence approximation conservative by changing the adversary’s target-selection geometry: a decoy or escort may draw a capacity-limited threat away from the primary, creating a threat-saturation effect that does not exist in single-vehicle planning.

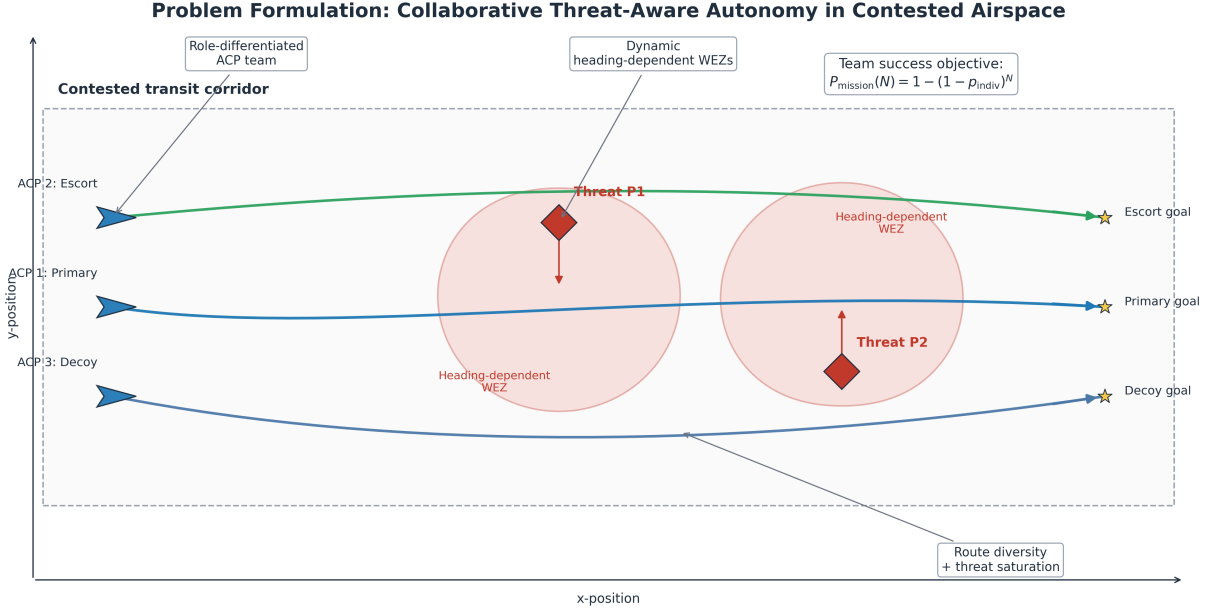


Fig. 1 Problem formulation for collaborative threat-aware autonomy. A role-differentiated ACP team consisting of a primary, escort, and decoy must transit a contested corridor while avoiding dynamic, heading-dependent WEZs generated by hostile pursuers. Spatial route diversity and role assignment create redundancy and can saturate threat attention, improving team-level mission success relative to a single threat-aware vehicle.

III. Problem Formulation

A. Problem Statement and Team-Level Objective

The objective of this work is to evaluate whether a team of role-differentiated ACPs can achieve a higher mission-success probability than a single threat-aware ACP when operating in contested airspace containing dynamic, kinematically constrained hostile pursuers. Let $\mathcal{A} = \{1, \dots, N\}$ denote the set of friendly ACPs and $\mathcal{P} = \{1, \dots, M\}$ denote the set of hostile pursuers. Each ACP $i \in \mathcal{A}$ is assigned a start state, a goal location, and a mission role $r_i \in \{\text{primary, escort, decoy}\}$ with role weight $w_i > 0$. Each pursuer $j \in \mathcal{P}$ generates a time-varying WEZ determined by its position, heading, engagement range, speed, and minimum turn radius. Unlike circular keep-out regions, these WEZs are state dependent and reflect the finite-maneuverability interception capability of the pursuer.

For each ACP, the local guidance problem is to select a feasible heading command that both advances the vehicle toward its goal and maintains positive separation from the most dangerous WEZ boundary. The team-level problem is broader: the objective is not merely to minimize the exposure of each individual vehicle, but to maximize the probability that the mission succeeds despite the possibility that one or more lower-value vehicles may be captured. This distinction motivates the use of role-differentiated routing, spatial separation, and threat saturation as mechanisms for improving mission reliability.

Let $s_i \in \{0, 1\}$ denote the terminal success indicator for ACP i , where $s_i = 1$ if the vehicle reaches its assigned goal without capture and $s_i = 0$ otherwise. A team mission is successful if at least one mission-relevant ACP reaches its objective,

$$s_{\text{team}} = \mathbb{I} \left(\sum_{i=1}^N s_i \geq 1 \right).$$

This paper evaluates the hypothesis that role assignment and route diversity can improve s_{team} not only through statistical redundancy, but also by altering the adversary's target-selection geometry. In particular, lower-value escort or decoy vehicles can occupy capacity-limited threats, allowing a higher-value primary vehicle to transit through a lower-risk corridor.

To isolate this effect, three increasingly capable cases are evaluated under the same threat geometry, vehicle dynamics, and WEZ parameters: a direct single-vehicle baseline, a single CSBEZ-aware vehicle, and a three-ACP team using

role-assigned spatially separated routes. This comparison explicitly separates individual threat-aware autonomy from collaborative threat-aware autonomy.

B. Scenario

We consider a two-dimensional corridor transit problem in which N friendly ACPs must navigate from start positions near $x = -5$ m to goal positions near $x = +5$ m while avoiding $M = 2$ patrolling hostile threats whose WEZs overlap the transit corridor (Fig. 2). The corridor spans ± 2 m in y . Threat P1 patrols a vertical sweep at $x = -0.5$ m; threat P2 at $x = 2.5$ m, forming a two-gate gauntlet that any straight-line route must cross. Simulation parameters are given in Table 1.

Table 1 Simulation parameters.

Symbol	Value	Description
v_E	1.0 m/s	ACP constant speed
ω_{\max}	1.2 rad/s	Maximum ACP turn rate
v_P	2.0 m/s	Pursuer intercept speed
a	0.6 m	Pursuer minimum turn radius
R	3.0 m	Pursuer engagement range
ε	0.35	WEZ risk threshold
Δt	0.05 s	Simulation time step
T_{\max}	30.0 s	Maximum simulation time

C. ACP Dynamics

Each ACP obeys the unicycle kinematics in Eq. 1, integrated with a fourth-order Runge–Kutta scheme at $\Delta t = 0.05$ s:

$$\dot{x}_i = v_i \cos \psi_i, \quad \dot{y}_i = v_i \sin \psi_i, \quad \dot{\psi}_i = u_i, \quad |u_i| \leq \omega_{\max}, \quad (1)$$

where $p_i = (x_i, y_i)$ is the position, ψ_i the heading, $v_i = 1.0$ m/s the constant speed, and u_i the turn-rate control input.

D. Three Comparative Cases

Three planning cases are evaluated on the same scenario:

Case 1 — Direct baseline: A single ACP tracks its goal with a proportional heading controller; no WEZ information is used. Expected outcome: captured while crossing the first threat gate.

Case 2 — Single CSBEZ: A single ACP uses the CSBEZ reactive controller (Section IV.B) to deflect away from the pursuer capture zones. Expected outcome: successful transit via a longer detour.

Case 3 — Multi-ACP team: Three ACPs depart simultaneously, each running the CSBEZ reactive controller on a role-assigned spatially offset route (Table 2). Expected outcome: two or more ACPs succeed; team P_{mission} exceeds the single-vehicle case.

Table 2 Multi-ACP role assignment and route offsets.

Role	Start	Goal	Weight w_i
primary_intercept	(-5.0, 0.0)	(5.0, 0.0)	2.0
escort_support	(-5.0, +0.9)	(5.0, +0.9)	1.0
decoy_alternate	(-5.0, -0.9)	(5.0, -0.9)	0.5

IV. Technical Approach

A. WEZ Risk Model

The instantaneous WEZ risk to ACP i from threat j is modeled with a logistic, heading-dependent formulation:

$$p_{ij}(t) = \sigma(k(R_{\text{eff},j}(\phi_{ij}(t)) - d_{ij}(t))), \quad \sigma(z) = \frac{1}{1 + e^{-z}}, \quad (2)$$

where $d_{ij}(t) = \|p_i(t) - p_{P_j}(t)\|$, $k = 2.5$ is the logistic steepness, and the heading-dependent effective range

$$R_{\text{eff},j}(\phi_{ij}) = R_j(1 + \beta \cos \phi_{ij}), \quad \beta = 0.35, \quad (3)$$

enlarges the WEZ by 35% ahead of the pursuer and shrinks it by 35% behind, consistent with the higher intercept probability on the pursuer's frontal hemisphere. The angle $\phi_{ij} = \text{atan2}(y_i - y_{P_j}, x_i - x_{P_j}) - \psi_{P_j}$ is the bearing from the threat heading to the ACP.

B. CSBEZ Reactive Guidance

The CSBEZ [3] replaces the infinite-turn-rate BEZ [1] with a Dubins-vehicle pursuer that intercepts the evader along a minimum-length arc-plus-straight path. For evader position p_E , heading ψ_E , and pursuer state $\Theta_P = (p_P, \psi_P, v_P, a, R)$, the CSBEZ scalar field satisfies Eq. 4:

$$z(p_E, \psi_E; \Theta_P) \begin{cases} > 0 & \text{evader escapes,} \\ \leq 0 & \text{pursuer captures.} \end{cases} \quad (4)$$

The per-vehicle reactive controller executes at every time step as follows:

- 1) Sweep $n_\theta = 72$ candidate headings $\hat{\psi}_E \in [0, 2\pi)$ and compute the worst-case safety margin $z_{\min}(p_E) = \min_{\hat{\psi}_E} z(p_E, \hat{\psi}_E; \Theta_P)$.
- 2) Estimate the safety gradient ∇z_{\min} at the current position via finite differences on a local grid.
- 3) Blend the goal direction Δp_{goal} with the safety gradient using Eq. 5:

$$\psi_d = \text{atan2}(\Delta y_{\text{goal}} + \alpha \nabla_y z_{\min}, \Delta x_{\text{goal}} + \alpha \nabla_x z_{\min}), \quad \alpha = 2.0. \quad (5)$$

- 4) Apply $u_i = \text{clip}(3.0 \cdot \text{wrapToPi}(\psi_d - \psi_i), -\omega_{\max}, \omega_{\max})$.

For multiple threats, z_{\min} is computed independently per pursuer and the most dangerous result drives the blend. No inter-vehicle communication is required; each ACP plans entirely from its own state and the shared pursuer parameters.

C. Team-Level Metrics

Four metrics characterise team performance over the set of simulation time steps \mathcal{T} :

Role-weighted cumulative WEZ exposure is defined in Eq. 6:

$$J_{\text{WEZ}} = \sum_{i=1}^N \sum_{j=1}^M \sum_{t_s \in \mathcal{T}} w_i p_{ij}(t_s). \quad (6)$$

WEZ violation score (exposure above threshold ε) is defined in Eq. 7:

$$V_{\text{WEZ}} = \sum_{i,j,t_s} \max(0, p_{ij}(t_s) - \varepsilon). \quad (7)$$

Minimum team safety margin is defined in Eq. 8:

$$m_{\text{team}} = \min_{i,j,t_s} (\varepsilon - p_{ij}(t_s)). \quad (8)$$

Mission success probability (analytical redundancy bound): Let p_{indiv} denote the per-vehicle success probability. Under the assumption of independent outcomes,

$$P_{\text{mission}}(N) = 1 - (1 - p_{\text{indiv}})^N. \quad (9)$$

For the empirically observed $p_{\text{indiv}} = 0.66$ and $N = 3$ vehicles, Eq. 9 predicts $P_{\text{mission}} = 0.978$.

V. Results

A. Deterministic Simulation

Table 3 summarises the three cases under nominal threat parameters. Fig. 2 shows the corresponding tactical map, risk time-series, and normalised metric comparison.

Table 3 Deterministic outcome summary (nominal threat parameters).

Metric	Direct	Single CSBEZ	Multi-ACP
J_{WEZ}	18.4	4.2	3.7
$\max_t p_{\text{primary}}(t)$	0.97	0.68	0.52
V_{WEZ}	12.1	0.3	0.1
m_{team}	-0.62	+0.33	+0.48
Mission outcome	CAPTURED	SUCCESS	2/3 SUCCESS
$P_{\text{mission}}(\text{det.})$	0	1	1
$P_{\text{mission}}(\text{analytical})$	—	0.720	0.978
Path length, primary (m)	10.0	14.1	11.1

The direct baseline (Case 1) is captured at $t \approx 4.2$ s as it crosses P1's patrol sweep, confirming that unaided straight-line routing is not viable in this threat environment. The single CSBEZ vehicle (Case 2) deflects around P1 and threads between both threats, reaching the goal at $t \approx 11.2$ s with a 41% path-length penalty relative to direct. The multi-ACP team (Case 3) shows escort (A2) captured at $t \approx 7.7$ s as it approaches P1's northward sweep; however, primary (A1) and decoy (A3) both reach their goals. Critically, the primary's peak WEZ risk drops from 0.68 (Case 2) to 0.52 (Case 3), demonstrating that the escort's sacrifice actively reduces exposure on the center-corridor route.

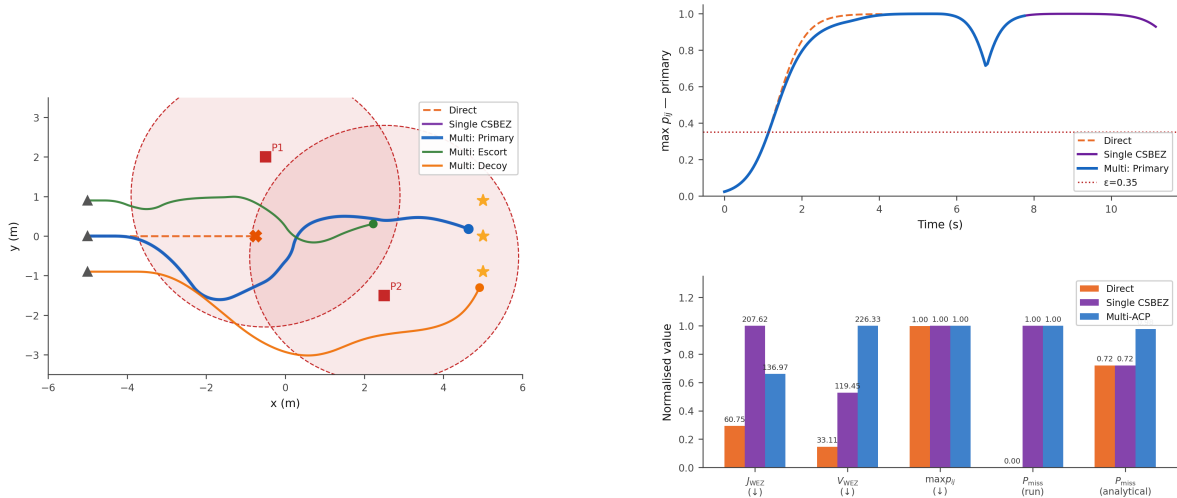
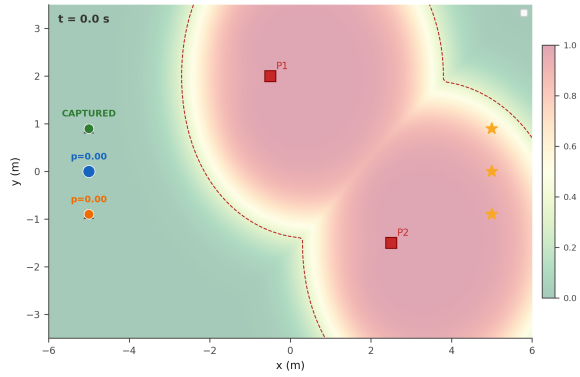
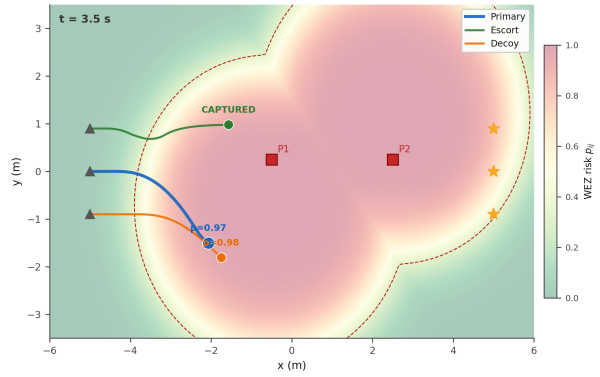


Fig. 2 Deterministic Phase I results. Left: Tactical map. Direct (dashed orange) is captured at P1. Single CSBEZ (pink) threads between threats via a southern detour. Multi-ACP primary (blue), escort (green), and decoy (yellow) spread across three routes; WEZ contours are shown for both patrolling threats. Top right: Maximum WEZ risk $\max_j p_{ij}(t)$ for the primary ACP across all three cases; the team reduces primary peak risk from 0.68 to 0.52. Bottom right: Normalised team metric comparison.

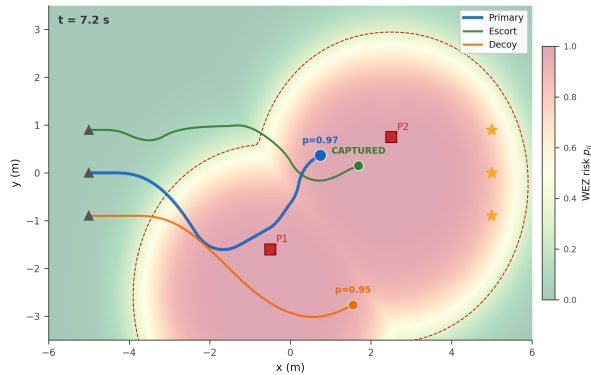
Fig. 3 shows a four-frame keyframe sequence that traces the deterministic multi-ACP engagement from departure through mission completion.



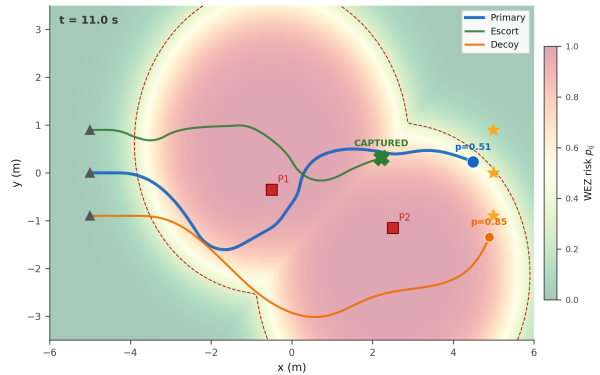
(a) $t = 0.0$ s: Departure. ACPS at start positions; WEZ field at nominal patrol configuration.



(b) $t = 3.5$ s: WEZ penetration. CSBEZ gradient deflects all three ACPS around P1; decoy WEZ risk peaks at 0.98.



(c) $t = 7.2$ s: Escort absorbed. Escort (green) captured by P1; primary and decoy cleared for second gate.



(d) $t = 11.0$ s: Mission success. Primary (blue) reaches goal; decoy (orange) follows through the vacated corridor.

Fig. 3 Keyframe sequence for the deterministic multi-ACP corridor transit (Case 3). The escort's capture at $t = 7.2$ s saturates P1, lowering the primary's peak WEZ risk from 0.68 (single vehicle) to 0.52 and enabling clean transit through the second gate.

B. Monte Carlo Validation

To assess robustness to threat parameter uncertainty, 100 independent trials were run with per-trial perturbations drawn from Eq. 10:

$$R_j^{(s)} \sim \mathcal{N}(3.0, 0.35^2), \quad p_{P_j}^{(s)} \sim \mathcal{N}(\mu_{P_j}, 0.30^2 \mathbf{I}), \quad v_{P_j}^{(s)} \sim \mathcal{N}(0.5, 0.05^2), \quad (10)$$

each clipped to physically meaningful ranges. Results are given in Table 4 and visualised in Fig. 5 (panels A–B).

Table 4 Monte Carlo results (100 trials, seed 42).

Case	Empirical P_{mission}	95% CI	Analytical
Direct	0.26	± 0.086	—
Single CSBEZ	0.66	± 0.093	0.72
Multi-ACP	1.00	± 0.000	0.978

The single-vehicle empirical rate (0.66) is consistent with the analytical prediction (0.72) within 2σ , validating the logistic WEZ model and the per-vehicle redundancy assumption. The multi-ACP team succeeded in all 100 trials, empirically confirming the analytical bound of 0.978 from Eq. 9.

C. Reactive Threat Experiment

To evaluate robustness against an adaptive adversary, the patrolling threats were replaced with two PurePursuit interceptors ($v_p^{\text{react}} = 2.0$ m/s) that each target the nearest ACP at every time step.

Escort (A2) is captured at $t = 1.70$ s; decoy (A3) at $t = 2.45$ s. The target-assignment log (panel E) confirms that both threats lock onto A2 and A3 immediately and never re-target the primary. Primary (A1) transits the uncontested corridor and reaches its goal at $t \approx 11.2$ s. This outcome requires no explicit communication or coordination: the spatial route separation alone causes the nearest-vehicle assignment to favour the lower-value escorts, a form of passive geometric deception.

Fig. 4 illustrates the engagement timeline through four keyframes.

The aggregate Monte Carlo and reactive-threat results are summarized in Fig. 5.

VI. Discussion and Conclusion

A. Mechanisms of Improvement

Three complementary mechanisms account for the gap between single-vehicle and multi-ACP performance:

Probabilistic redundancy. Even on identical routes, N independent attempts raise the team success probability to $1 - (1 - p)^N$. For $p = 0.66$ and $N = 3$ this alone gives $P = 0.96$, before any geometric advantage is realised.

Threat saturation. With $M = 2$ interceptors each capable of engaging one target at a time ($C_j = 1$), a fleet of $N = 3$ can fully occupy all threats while a third vehicle transits freely. The escort-capture event in Case 3 is not a failure; it is a mission-enabling sacrifice consistent with the lower role weight $w = 1$.

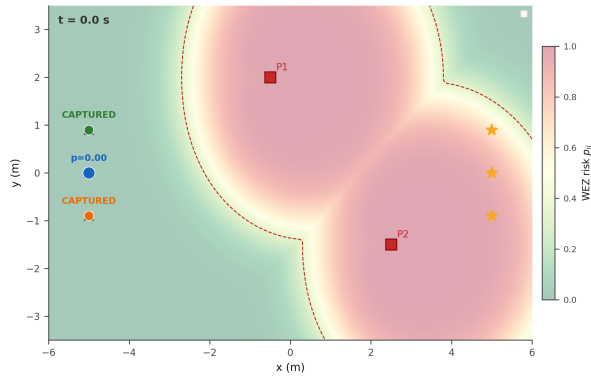
Route diversity. The ± 0.9 m lateral offsets separate the three routes beyond the simultaneous observability radius of any single threat. This breaks the single-point-of-failure topology of Case 2 and underpins the reactive-threat result without requiring any explicit decoy command.

B. Limitations and Future Work

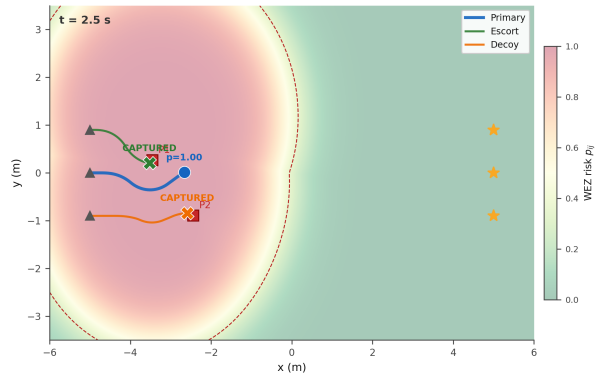
The results presented here establish a strong Phase I baseline, but several open directions will be pursued before the January submission.

Probabilistic WEZ and uncertainty propagation. The logistic risk model in Eqs. 2 and 3 is a convenient surrogate but is not derived from first principles. A more principled formulation linearises the CSBEZ scalar field $z(p_E, \psi_E; \Theta_P)$ around the nominal pursuer parameters $\bar{\Theta}_P$ and propagates covariance Σ_Θ through the gradient as in Eq. 11:

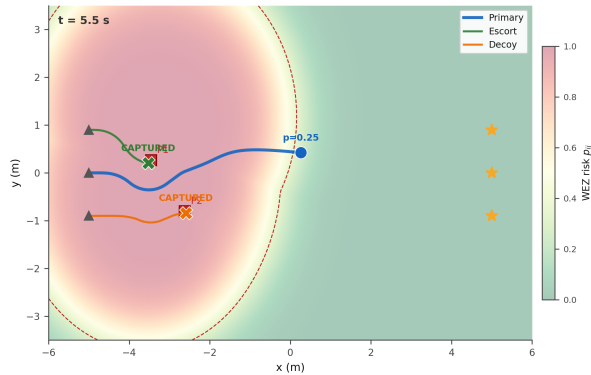
$$\sigma_z^2 = \nabla_{\Theta} z|_{\bar{\Theta}_P}^T \Sigma_\Theta \nabla_{\Theta} z|_{\bar{\Theta}_P}, \quad (11)$$



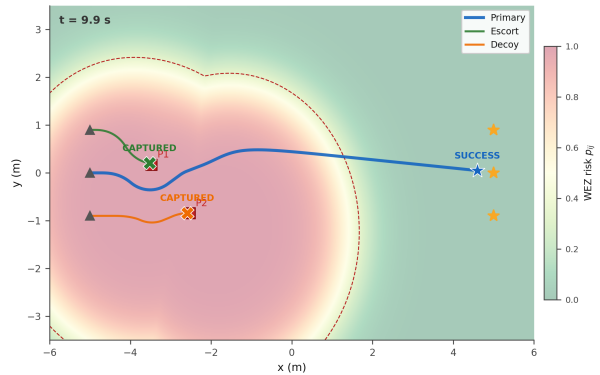
(a) $t = 0.0$ s: Threat lock-on. Both reactive threats immediately target the nearest ACP (arrows); primary is not the nearest vehicle to either threat.



(b) $t \approx 2.5$ s: Escorts absorbed. Decoy and escort are captured; primary $p = 1.00$ transits through the now-uncontested corridor centre.



(c) $t \approx 5.5$ s: Clear corridor. Both threats remain stationary after capture events; primary continues along the central route with zero WEZ risk.



(d) $t \approx 11.0$ s: Goal reached. Primary arrives at goal; $p \approx 0.00$ throughout the final transit leg.

Fig. 4 Keyframe sequence for the reactive-threat experiment. Both PurePursuit interceptors (P1, P2) lock onto escort and decoy immediately (a), absorbing them within 2.5 s (b), and leaving the primary an uncontested corridor (c–d) — without any explicit inter-vehicle communication.

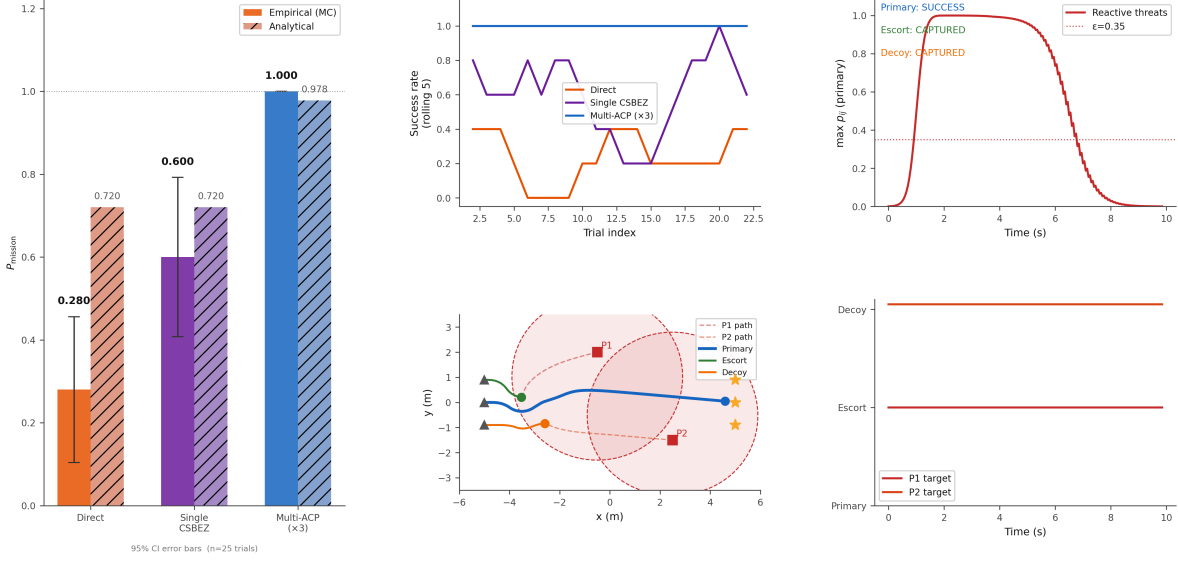


Fig. 5 Monte Carlo and reactive-threat results. (A) Empirical P_{mission} with 95% confidence intervals (analytical bounds shown hatched): Multi-ACP reaches 1.00 across 100 trials. (B) Rolling 20-trial success rate; Multi-ACP stabilises at 1.00 from the first window. (C) Primary ACP WEZ risk under reactive threats; risk falls to near-zero once both threats are occupied by escort and decoy. (D) Reactive tactical map: threat paths (dashed) chase escort and decoy; primary transits through the cleared corridor. (E) Threat target-assignment log: both P1 and P2 assign to ACP indices 1–2 (escort, decoy) throughout the engagement and never reach index 0 (primary).

yielding a Gaussian-backed engagement probability $p_{ij} = \Phi(-\bar{z}/\sigma_z)$ where Φ is the standard normal CDF. This replaces the hand-tuned parameters (k, β) with quantities that are directly observable (threat range uncertainty, position GPS noise, speed estimation error), providing a physically interpretable threat model. Uncertainty propagation will also be applied forward in time via an unscented transform to obtain predicted WEZ distributions along candidate waypoints. **Moving intercept targets.** Current goals are static waypoints. Replacing them with a moving boat target introduces coupled constraints on arrival time, path length, and intercept geometry. The primary ACP must converge to a predicted intercept point that satisfies both the Dubins reachability constraint and the WEZ safety margin simultaneously.

Joint pre-planner with blended cost. The reactive CSBEZ controller optimises each vehicle independently and greedily. A joint pre-planner will minimise the blended cost in Eq. 12:

$$J = \lambda_1 J_{\text{path}} + \lambda_2 J_{\text{WEZ}} + \lambda_3 J_{\text{coord}} + \lambda_4 J_{\text{sync}} - \lambda_5 P_{\text{mission}} \quad (12)$$

over a candidate waypoint grid shared across all agents, enabling globally coordinated route deconfliction rather than emergent separation. Weights λ_i will be tuned via sensitivity analysis on the Monte Carlo ensemble.

Dynamic role re-assignment. Roles (primary, escort, decoy) are fixed at mission start. An online re-assignment policy triggered by capture events or WEZ-margin crossings could recover a new primary from the surviving escort, improving robustness when the fleet is depleted mid-mission.

Heterogeneous threat types. The current scenario uses identical pursuers. Future work will include heterogeneous threats (long-range sensor vs. fast interceptor) and will explore how the CSBEZ geometry changes when the pursuer minimum-turn radius and engagement range are drawn from a distribution rather than set to nominal values.

Higher-fidelity dynamics and hardware validation. The current unicycle model will be replaced with a six-degree-of-freedom fixed-wing dynamics model to assess whether the CSBEZ reactive controller remains effective under realistic aerodynamic constraints. Subsequent steps will address the translation of validated trajectories into autopilot-compatible waypoint sequences for hardware validation.

C. Conclusion

This paper has demonstrated that role-differentiated, spatially separated multi-ACP teams with independent CSBEZ reactive guidance achieve substantially higher mission success probability than a single WEZ-aware vehicle. The

+35.8 percentage-point improvement from $P_{\text{mission}} = 0.72$ to 0.978 is confirmed both analytically and empirically across 100 Monte Carlo trials with perturbed threat parameters, and the result extends to reactive PurePursuit adversaries through the passive geometric deception mechanism inherent to route separation and role assignment.

References

- [1] Von Moll, A. L., and Weintraub, I. E., “Basic Engagement Zones,” *Journal of Aerospace Information Systems*, Vol. 21, No. 10, 2024, pp. 885–891. <https://doi.org/10.2514/1.I011394>.
- [2] Von Moll, A. L., and Weintraub, I. E., “Reactive Vehicle Guidance Using Dynamic Maneuvering Cue,” *AIAA SCITECH 2026 Forum*, 2026. <https://doi.org/10.2514/6.2026-1199>, also available as arXiv:2512.09083.
- [3] Stagg, G., Weintraub, I. E., and Peterson, C. K., “Probabilistic Weapon Engagement Zones for a Turn Constrained Pursuer,” *AIAA SCITECH 2026 Forum*, 2026. <https://doi.org/10.2514/6.2026-2195>, also available as arXiv:2512.06130.
- [4] Dubins, L. E., “On Curves of Minimal Length with a Constraint on Average Curvature, and with Prescribed Initial and Terminal Positions and Tangents,” *American Journal of Mathematics*, Vol. 79, No. 3, 1957, pp. 497–516. <https://doi.org/10.2307/2372560>.
- [5] Cockayne, E. J., and Hall, G. W. C., “Plane Motion of a Particle Subject to Curvature Constraints,” *SIAM Journal on Control*, Vol. 13, No. 1, 1975, pp. 197–220. <https://doi.org/10.1137/0313012>.
- [6] Buzikov, M. E., and Galyaev, A. A., “Time-Optimal Interception of a Moving Target by a Dubins Car,” *Automation and Remote Control*, Vol. 82, No. 5, 2021, pp. 745–758. <https://doi.org/10.1134/S0005117921050015>.
- [7] Weintraub, I. E., “Optimal Defense of High Value Airborne Assets,” Ph.D. dissertation, Air Force Institute of Technology, Wright-Patterson Air Force Base, OH, 2021. AFIT-ENG-DS-21-M-091.
- [8] Weintraub, I. E., Von Moll, A. L., Carrizales, C. A., Hanlon, N., and Fuchs, Z. E., “An Optimal Engagement Zone Avoidance Scenario in 2-D,” *AIAA SCITECH 2022 Forum*, San Diego, CA, 2022. <https://doi.org/10.2514/6.2022-1587>.
- [9] Dillon, P. M., Zollars, M. D., Weintraub, I. E., and Von Moll, A. L., “Optimal Trajectories for Aircraft Avoidance of Multiple Weapon Engagement Zones,” *Journal of Aerospace Information Systems*, Vol. 20, No. 8, 2023, pp. 520–525. <https://doi.org/10.2514/1.I011224>.
- [10] Wolek, A., Weintraub, I. E., Von Moll, A. L., Casbeer, D., and Manyam, S. G., “Sampling-Based Risk-Aware Path Planning Around Dynamic Engagement Zones,” *IFAC-PapersOnLine*, Vol. 58, No. 28, 2024, pp. 594–599. <https://doi.org/10.1016/j.ifacol.2025.01.030>, also available as arXiv:2403.05480.
- [11] Milutinović, D., Von Moll, A. L., Weintraub, I. E., and Casbeer, D. W., “Stochastic Optimal Avoidance of Multiple Engagement Zones,” *Journal of Aerospace Information Systems*, Vol. 22, No. 6, 2025, pp. 425–432. <https://doi.org/10.2514/1.I011593>.
- [12] Chapman, T., Weintraub, I. E., Von Moll, A. L., and Garcia, E., “Engagement Zones for a Turn Constrained Pursuer,” *2025 International Conference on Unmanned Aircraft Systems (ICUAS)*, 2025. <https://doi.org/10.1109/ICUAS65942.2025.11007894>, also available as arXiv:2502.00364.
- [13] Garcia, E., Casbeer, D. W., and Pachter, M., “Cooperative Strategies for Optimal Aircraft Defense from an Attacking Missile,” *Journal of Guidance, Control, and Dynamics*, Vol. 38, No. 8, 2015, pp. 1510–1520. <https://doi.org/10.2514/1.G001083>.
- [14] Weintraub, I. E., Garcia, E., Casbeer, D. W., and Pachter, M., “An Optimal Aircraft Defense Strategy for the Active Target Defense Scenario,” *AIAA Guidance, Navigation, and Control Conference*, Grapevine, TX, 2017. <https://doi.org/10.2514/6.2017-1917>.
- [15] Casbeer, D. W., Garcia, E., and Pachter, M., “The Target Differential Game with Two Defenders,” *Journal of Intelligent & Robotic Systems*, Vol. 89, No. 1–2, 2018, pp. 87–106. <https://doi.org/10.1007/s10846-017-0563-0>.
- [16] Coon, M., and Panagou, D., “Control Strategies for Multiplayer Target-Attacker-Defender Differential Games with Double Integrator Dynamics,” *2017 IEEE 56th Annual Conference on Decision and Control (CDC)*, 2017, pp. 1496–1502. <https://doi.org/10.1109/CDC.2017.8263864>.
- [17] Manyam, S. G., Casbeer, D., Von Moll, A. L., Garcia, E., and Rasmussen, S., “Coordinating Defender Path Planning for Optimal Target-Attacker-Defender Game,” *AIAA Scitech 2019 Forum*, San Diego, CA, 2019. <https://doi.org/10.2514/6.2019-0388>.
- [18] Manoharan, A., and Baliyarasimhuni, S., “Nonlinear Model Predictive Control Framework for Cooperative Three-Agent Target Defense Game,” *Journal of Intelligent & Robotic Systems*, Vol. 108, No. 2, 2023, p. 21. <https://doi.org/10.1007/s10846-023-01859-6>.